Solar and Thermal Radiation Errors on Upper-Air Radiosonde Temperature Measurements

R. PHILIPONA

Federal Office of Meteorology and Climatology (MeteoSwiss), Payerne, Switzerland

A. KRÄUCHI

Institute for Atmospheric and Climate Science, ETH Zurich, Zurich, Switzerland

G. ROMANENS AND G. LEVRAT

Federal Office of Meteorology and Climatology (MeteoSwiss), Payerne, Switzerland

P. RUPPERT

Meteolabor AG, Wetzikon, Switzerland

E. BROCARD, P. JEANNET, D. RUFFIEUX, AND B. CALPINI

Federal Office of Meteorology and Climatology (MeteoSwiss), Payerne, Switzerland

(Manuscript received 12 February 2013, in final form 22 April 2013)

ABSTRACT

Atmospheric temperature and humidity profiles are important for weather prediction, but climate change has increased the interest in upper-air observations asking for very high-quality reference measurements. This paper discusses an experimental approach to determine the radiation-induced error on radiosonde air temperature measurements. On the one hand, solar shortwave and thermal longwave radiation profiles were accurately measured during radiosonde ascents from the surface to 35-km altitude. On the other hand, air temperature was measured with several thermocouples on the same flight, simultaneously under sun-shaded and unshaded conditions. The radiation experiments reveal that thermal radiation errors on the very thin thermocouple of the Meteolabor SRS-C34 radiosonde are similar during night- and daytime. They produce a radiative cooling in the lower troposphere and the upper stratosphere, but a radiative heating in the upper troposphere and lower stratosphere. Air temperature experiments with several thermocouples, however, show that solar radiation produces a radiative heating of about +0.2°C near the surface, which linearly increases to about +1°C at 32 km (~10 hPa). The new solar radiation error profile was then applied to SRS-C34 measurements made during the Eighth WMO Intercomparison of High Quality Radiosonde Systems, held in Yangjiang, China, in July 2010. The effects of thermal and solar radiation errors are finally shown in contrast to the 10 other internationally used radiosonde systems, which were flown during this international campaign.

1. Introduction

Atmospheric temperature and water vapor measurements have been used in a wide variety of both operational weather prediction and research applications for many years. However, upper-air observations for climate have recently been given more attention with the initiation of the Global Climate Observing System (GCOS) Reference Upper Air Network (GRUAN) to provide climate-quality measurements of tropospheric and lower-stratospheric variables (Trenberth et al. 2002; GCOS 2007; Seidel et al. 2009). GRUAN's goal is to feature measurements of the "essential climate variables" identified by GCOS (GCOS 2010) with a focus on upper-air variables. The primary objectives are to monitor changes

Corresponding author address: Rolf Philipona, Federal Office of Meteorology and Climatology (MeteoSwiss), Chemin de l'Aerologie 1, CH-1530 Payerne, Switzerland.
E-mail: rolf.philipona@meteoswiss.ch

DOI: 10.1175/JTECH-D-13-00047.1

© 2013 American Meteorological Society

in temperature profiles and to characterize water vapor in the upper troposphere and lower stratosphere (UTLS) (Thorne et al. 2005; Randel et al. 2006).

The measurement quality of present-day operational radiosondes is best described in a recent report on the Eighth World Meteorological Organization (WMO) Intercomparison of High Quality Radiosonde Systems, held in Yangjiang, China, in July 2010 (Nash et al. 2011). During this intercomparison, 11 operational radiosonde systems from 11 manufacturers were tested and compared in relation to temperature, humidity, pressure, and wind components. With respect to temperature profile measurements at night, most radiosonde systems were found to provide suitable quality for both weather and climate application. During daytime however, a rather large spread was found between the results of the individual sondes, particularly at high altitudes, with biases up to ±0.8°C at 32-km altitude (~10 hPa). A particular large cold bias of −0.8°C at high altitude was found for the Meteolabor SRS-C34 radiosonde (MeteoSwiss operational radiosonde), which uses a large daytime radiation error correction (−1.8°C at 32 km) that is based on laboratory experiments and on statistical analyses of day–night differences (Ruffieux and Joss 2003).

The large differences of daytime temperature measurements observed during the 2010 WMO intercomparison led us to reanalyze the radiation error of the Meteolabor SRS-C34 radiosonde. In the following, we present experiments that allow determining the thermal and solar radiation error of the thermocouple temperature sensors used on the SRS-C34 radiosonde. We show solar shortwave and thermal longwave radiation profiles measured through the atmosphere with radiosondes, which allow relating radiation errors on temperature sensors to the radiative fluxes. We further show an experimental method allowing direct measurements of the radiation error by using several thermocouples on the same sonde, which simultaneously measure air temperature under sun-shaded and unshaded conditions. The new radiation error correction is then applied to the SRS-C34 radiosonde, and we use the data of the 2010 WMO intercomparison to analyze and compare night and day measurement differences between the SRS-C34 and the 10 other internationally used radiosonde systems.

2. Radiation error of air temperature measurements

A large number of studies and tests on the problems of gas temperature measurements have been reported in the nineteenth century and first half of the twentieth century (Freeze 1951). It is generally known that the temperature, which a temperature sensor indicates, is not usually the temperature of the gas. It is a temperature that is a result of the rate of heat transfer from the gas and its surroundings to the sensor by radiation, balanced against the rate of heat transfer from the sensor by radiation and convection–conduction to the gas and surroundings, and by conduction from the sensor to its support. The factors that cause a sensor to indicate a temperature different from the gas temperature have been described as ''errors of the sensor'' (Daniels 1968).

With respect to air temperature measurements with radiosondes, a number of analyses on errors of sensors have been published (Vaisala 1964; Schmidlin et al. 1986; Luers 1990; McMillin et al. 1992; Luers 1997; Ruffieux and Joss 2003). The most prominent error of upper-air temperature sensors is the radiation-induced temperature error, or ''radiation error,'' which is related to the following three main causes:

1) Radiative transfer between the sensor and its surrounding objects, which have a temperature different from that of the air; for example, the sun, as a source hotter than the gas, will cause a thermometer to indicate too high a temperature, while a clear sky, as a source colder than the gas, will cause a thermometer to indicate too low a temperature.
2) Convective–conductive heat transfer between the sensor and the gas, which is the main process through which the temperature sensor approaches the gas temperature and this varies with pressure and with the speed of motion of the air across the sensor.
3) Construction of the sensor and its support itself, which influences the radiation error and causes additional errors. The surface emissivity/absorptivity of the sensor, on the one hand, is crucial with respect to the radiation error. Conductive heat transfer from the sensor to the sensor support, on the other hand, causes large errors on poorly designed air temperature measuring systems.

The three causes indicate that on atmospheric air temperature measurements, the radiation error changes with altitude—first, due to changing radiative fluxes; and second, due to decreasing pressure—and hence decreasing convective–conductive heat transfer between the sensor and the air. Many methods have been used to improve air temperature measurements. However, the most generally accepted methods—that is, reducing the size of the sensor, reducing the surface emissivity–absorptivity, and increasing the speed of the gas over the sensor (Daniels 1968)—are to this day always a compromise and only partially eliminate the error.

In our experiments we used the Meteolabor thermocouple temperature sensor, which to our knowledge is smaller than all other temperature sensors presently

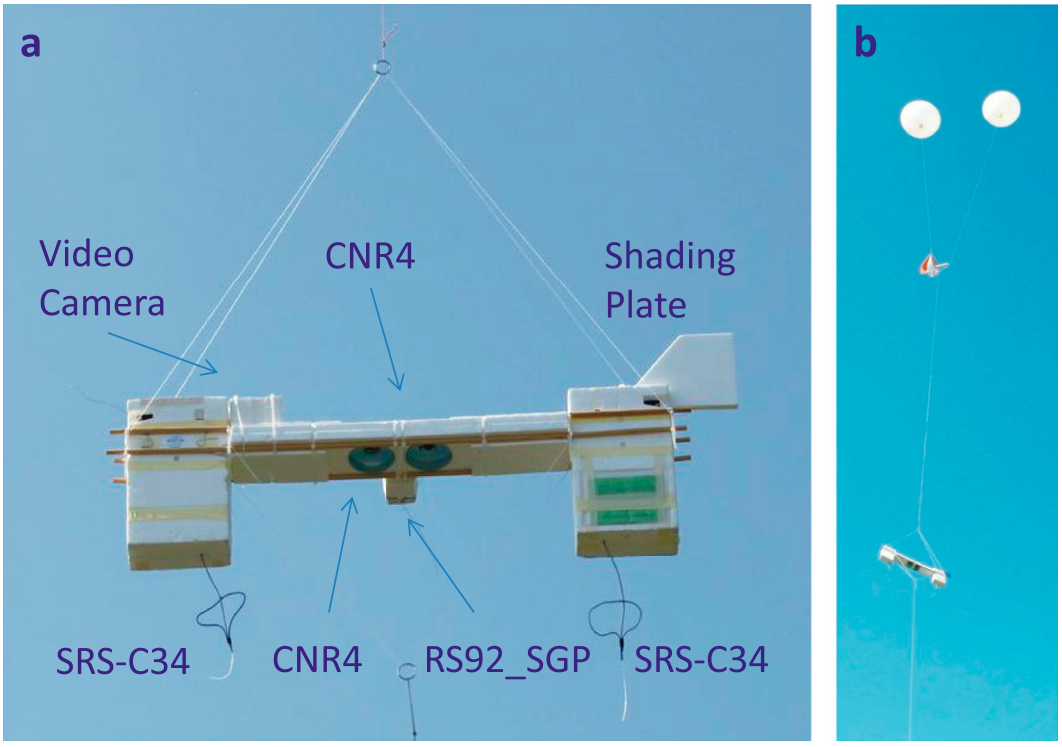

FIG. 1. (left) Radiosonde package to measure radiation flux profiles and air temperature under shaded and unshaded conditions and (right) double-balloon sounding. Two SRS-C34 radiosondes measure air temperature with several thermocouple sensors, as well as humidity and all signals from the CNR4 net radiometer. CNR4 is in the center measuring upward and downward solar and thermal radiation. Shading plate for measuring temperature in shaded conditions is mounted on the SRS-C34 on the right. The system is also equipped with a RS92-SGP radiosonde and a video camera.

used on operational radiosondes. As on most other radiosonde systems, we have only limited knowledge on the emissivity–absorptivity of the sensor head and the connecting wires, for the shortwave as well as for the longwave radiation. The ascent rate of the radiosonde during the experiments, and hence the ventilation, was the same as during standard operational radiosonde ascents. However, we measured the solar and thermal radiation fluxes downward and upward and measured the air temperature under sun-shaded and unshaded conditions during the same flight. This allowed us to directly measure the radiation error and relate it to the measured thermal and direct solar radiation.

3. Experimental setup

The experiments were made with a global positioning system (GPS)-equipped digital Meteolabor SRS-C34 radiosonde, which is fitted with several thermocouples to measure air temperature under shaded and unshaded conditions and has a capacitive polymer humidity sensor. A second SRS-C34 provides measuring channels to measure the signals of a modified Kipp & Zonen CNR4 net radiometer, which is used to measure shortwave and longwave radiation fluxes through the atmosphere (Philipona et al. 2012). The CNR4 net radiometer is mounted between the two SRS-C34 radiosondes (Fig. 1a). The sonde package also carries a Vaisala RS92-SGP radiosonde for temperature and humidity comparisons and a video camera to monitor the flight. We use a new flight technique with two balloons, which reduces pendulum motion and guarantees a more quiescent ascent and a controlled descent (Fig. 1b).

a. Air temperature measurement with thermocouples

The air temperature sensor used on the SRS-C34 was developed by Meteolabor AG and consists of a copper–constantan thermocouple, which is referenced to a high-precision custom-made copper resistance thermometer R measuring the temperature T_r inside the sonde (Fig. 2). The sensor measuring air temperature T is a soft-solder connection of a 64-μm copper and a 50-μm constantan wire, which are both about 5 cm long and extend from 300-μm copper and constantan wires. The solder connection is of similar size as the thin wires, hence less than 100 μm. Accurate measurements of the resistance R and

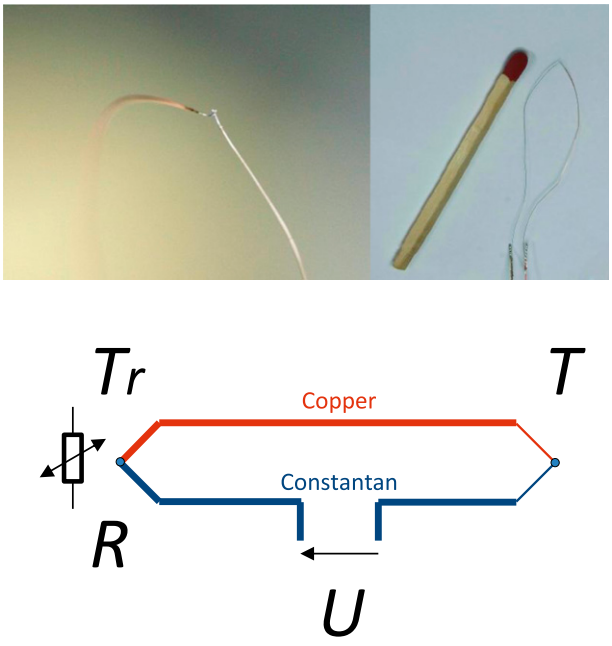

FIG. 2. Copper–constantan thermocouple sensor used on the SRS-C34 to measure T, which is referenced to R measuring T_r inside the sonde.

the voltage U, which are both measured by the same electronic circuit, allow determining the temperature inside the sonde T_r and T. All copper and constantan wires used for the thermocouple and the resistance thermometer are always from the same batch, which has been characterized at the Swiss bureau of standards, Federal Office of Metrology (METAS). Since the resistance of copper has a well-known quasi-perfect linear relation to temperature, the ''calibration'' of the individual sonde consists of a simple adjustment of the ambient temperature reading of the copper resistance thermometer by the radiosonde electronics to a METAS-traced reference thermometer. Thus, the temperature traceability chain is ensured essentially from the METAS reference down to the temperature sensor on board the SRS-C34. The adjustment is made by the manufacturer, and the prelaunch check only consists of a comparison of the radiosonde temperature reading to a reference thermometer at room temperature. The robust calibration also allows easy reuse of the sonde, which reduces costs and is a contribution to environmental protection.

b. *Shaded and unshaded air temperature measurements*

The specifically prepared SRS-C34, which has several thermocouples, is also equipped with a shading plate in the upper part on the right side of the sonde (Figs. 1 and 3). Shading plates of different material (aluminum and

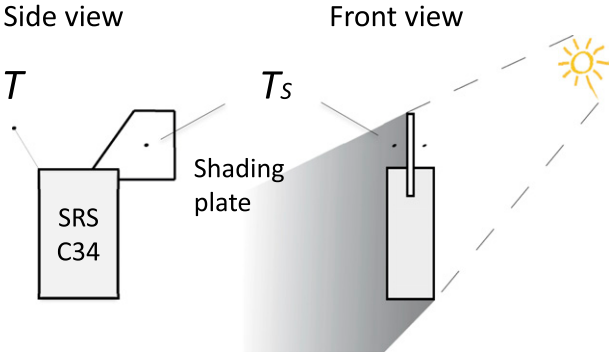

FIG. 3. Shading plate on Meteolabor SRS-C34 radiosonde for shading T_S, which are at a distance of 5 cm at each side of the shading plate; T_S measured in the shade is compared to T measured by the unshaded operational temperature sensor.

styrofoam) and different colors (aluminized, black, and white) have been used. All thermocouples are identical and referenced to the same resistance thermometer. The operational thermocouple, which measures T, is on the left side and unaffected by the shading plate (Fig. 3). On each side of the shading plate, a thermocouple is mounted at a distance of 5 cm and close to the center of the shading plate. During the ascent the sonde package is free to rotate, hence the temperature sensors T_S beside the shading plate are at times in the shade and at times exposed to the sun. Because of the large size of the sonde package, the rotation is rather slow and the very fast temperature sensors ($t_c < 300$ ms), which are sampled at 1-s resolution, can easily track the air temperature changes when the T_S are in the shade or in the sun. Hence, these experiments allow measuring the difference of the air temperature measured by the operational air temperature sensor, which is continuously exposed to direct solar radiation and the air temperature measured under direct sun-shaded conditions.

c. *Upper-air solar and thermal radiometry*

The CNR4 net radiometer consists of two pyranometers for measuring downward and upward solar shortwave radiation, and two pyrgeometers for measuring upward and downward thermal longwave radiation. The pyranometers and pyrgeometers thermopile voltages, and body and dome temperatures are measured by the second SRS-C34 radiosonde. Precise body and dome temperature measurements of the pyranometers and pyrgeometers are crucial. These measurements allow for corrections of differential thermal emissions between the radiometer domes and the thermopile, which result from large temperature gradients, when the instrument cools from +20°C at the surface down to −60°C in the stratosphere. The four radiometers are precalibrated and compared to surface radiation measurements at the

Payerne Baseline Surface Radiation Network (BSRN) station before launch. Measurement uncertainty is traced to BSRN standards, which is on the order of 1%, hence, $\pm(2\text{–}4)\,\mathrm{W\,m^{-2}}$ for longwave radiation and $\pm(4\text{–}8)\,\mathrm{W\,m^{-2}}$ for shortwave radiation. The CNR4 is kept as horizontal as possible during the flight, and the pyranometers and pyrgeometers measure solar and thermal irradiance from above and from below, respectively, in watts per meter squared (Philipona et al. 2012).

d. Double-balloon flight technique

A new technique is used to lift the radiosonde package for these experimental flights, consisting of two balloons and an aluminum triangle equipped with a GPS-controlled mechanism that allows automatic release of the larger carrier balloon at a preset altitude (Fig. 1b). The two balloons are inflated such as to lift the payload at a constant ascent rate of $5\text{–}7\,\mathrm{m\,s^{-1}}$ from the aerological station at Payerne (491 m) to above 30 km. During the 2-h ascent, the radiosonde makes a horizontal displacement of 30–50 km and transmits the measured signals at 1-s resolution to the ground. After the release of the carrier balloon, the sonde descends with the smaller parachute balloon at a similar speed as during ascent, which makes a second profile measurement possible. The double-balloon flight technique not only allows flight control but also strongly reduces the pendulum motion of the sonde and guaranties a smooth flight with reduced sonde rotation. The sondes are tracked by GPS technology and recovered and reused.

4. Radiative flux profiles and radiation error

Sensors measuring atmospheric temperature are subject to radiative fluxes from above and from below, which are balanced by the sensors' thermal radiative emission. Shortwave downward (SDR) and upward (SUR) radiation, as well as longwave downward (LDR) and upward (LUR) radiation, were measured under cloud-free situations during daytime (NAME_d) and night (NAME_n) on 23 September 2011 from the surface to about 32 km (Fig. 4a). Downward radiative fluxes are positive and upward fluxes negative and are given in watts per meter squared. SDR shows the vertical downward solar flux, whereas the direct solar irradiance (DIR) is the component normal to the light propagation using SDR. More detailed information on upper-air radiation measurements is given in Philipona et al. (2012).

a. Radiation errors on temperature sensors during nighttime

Figure 4b shows the night radiative fluxes that are absorbed and emitted by a temperature sensor shown as a sphere. Here, fluxes absorbed by the sphere are positive and fluxes emitted are negative. LDR_n and LUR_n are both positive fluxes because they are absorbed by the sensor from above and from below, respectively. However, the sensor, which is close to air temperature, emits radiation downward and upward according to the Stephan Boltzmann law multiplied by its surface emissivity ($\varepsilon\sigma T^4$) (see also section 4c). The sum of the absorbed and emitted fluxes result in the longwave radiation balance of the sensor during the night (LRB_n), which is negative in the lower troposphere, and then becomes positive and again negative further up in the stratosphere. Hence, in the lower troposphere, LRB_n cools the temperature sensor, higher up LRB_n warms the temperature sensor, and above 25 km it again cools the temperature sensor.

b. Radiation errors on temperature sensors during daytime

The longwave radiative impact on the sensor from above and from below is very similar during the day and during the night (Fig. 4c). The magnitude of LRB_d of about $-100\,\mathrm{W\,m^{-2}}$ in the troposphere and of about $+100\,\mathrm{W\,m^{-2}}$ in the stratosphere is representative of clear-sky situations throughout the year, but is smaller in the troposphere during cloudy situations. However, during daytime, direct solar radiation DIR from above and reflected solar radiation SUR from below produces an additional and considerably larger error on the temperature measurement (see chapter 7). Under cloud-free situations DIR increases in the troposphere and with more than $+1300\,\mathrm{W\,m^{-2}}$ reaches almost the solar constant at the tropopause, and shows only minor increases further up. SUR is considerably lower under cloud-free situations but can reach values of about $+500\,\mathrm{W\,m^{-2}}$ above highly reflective clouds.

c. Temperature sensor absorption and emission

As mentioned above, shortwave and longwave absorption and emission coefficients of the sensors are not well known. The radiation fluxes in Fig. 4 are shown as measured in the atmosphere. Thermal emission of the sensor is calculated with an emissivity coefficient of 1. Hence, the irradiances shown for LRB_n and LRB_d are calculated with sensor emissivity–absorptivity equal to 1. In reality, longwave absorptivity and emissivity are equal but rather between 0.4 and 0.8; hence, LNR_n and LNR_d need to be multiplied by the emissivity–absorptivity coefficient to get the correct magnitude, but the vertical distribution stays the same. Shortwave absorption is also considerably lower than 1; hence, a direct quantitative relation between radiation fluxes and temperature error cannot easily be done. However, the measurements allow a qualitative evaluation of the

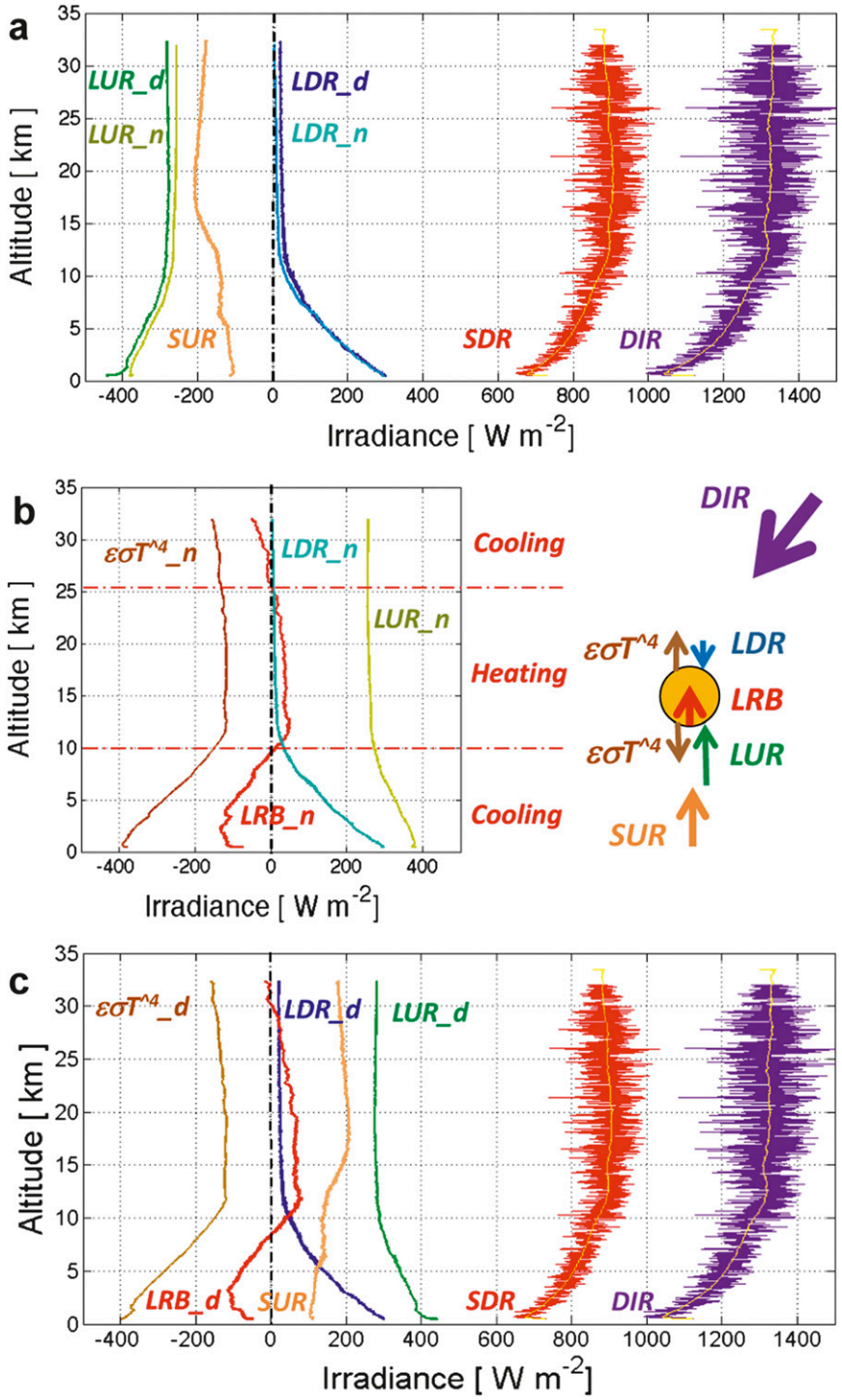

FIG. 4. Solar and thermal radiation flux profiles from the surface to 32-km altitude. (a) LUR and LDR for day and night, and SUR and SDR as well as direct solar radiation. (b) Thermal fluxes during the night and LRB on the temperature sensor. (c) Thermal fluxes and solar fluxes during daytime (adapted from Philipona et al. 2012).

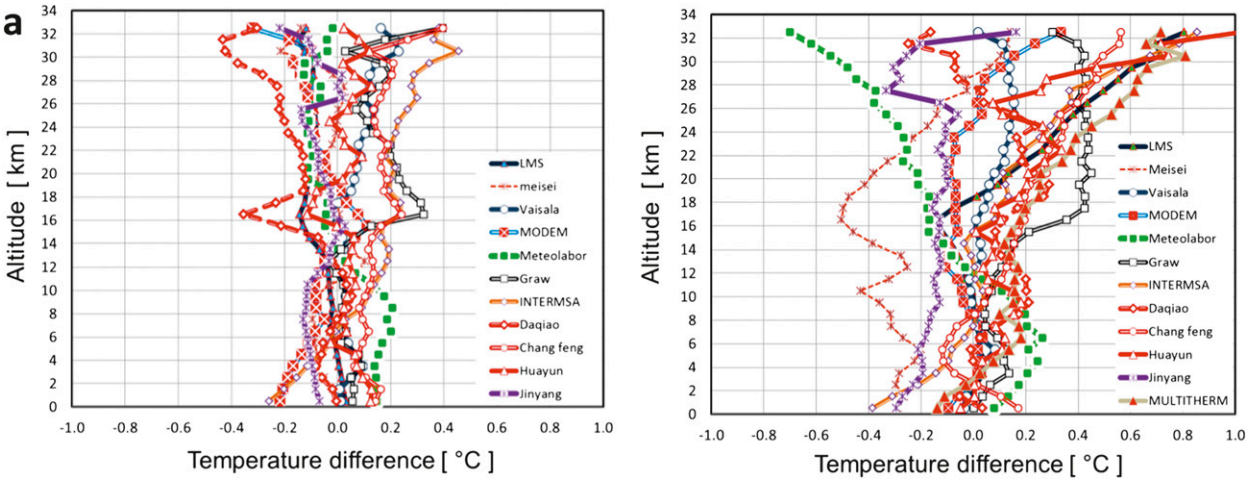

FIG. 5. Results of the 2010 WMO radiosonde intercomparison, which evaluated 11 operational radiosondes and the Sippican LMS-6 multithermistor (daytime only) for temperature, for (a) nighttime and (b) daytime (figures from Nash et al. 2011). Reference that defines zero temperature differences is the average of four radiosondes, as discussed in the text.

vertical distribution of the radiative impact and demonstrate longwave cooling at the bottom and the top and warming around the tropopause, and shortwave warming increasing with altitude.

5. Status of upper-air temperature measurements

The 2010 WMO radiosonde intercomparison in Yangjiang, China, evaluated 11 operational radiosondes and the Sippican LMS-6 multithermistor (daytime only) for temperature (Nash et al. 2011). The 11 instruments were flown in two groups. Group working references were determined, which were part of most flights in a group, and have good measurement quality. The LMS system was used as group working reference in one group, whereas the Meisei system was used as working reference in the other group. The linking between the two groups was made with the help of Vaisala, Meteolabor, Daqiao, and Multithermistor measurements. Temperature comparison statistics were computed for simultaneous samples, banded into layers 1 km thick from the surface to 33 km using the RSKOMP software suite. Statistical analysis was used to estimate systematic and random errors, day–night differences, time response, and other characteristics of each sensor. For the systematic night biases (Fig. 5a), at least 15 successful comparison flights of each type to 26 km, 8 flights to 29 km, and 5 flights to 33 km were used. The systematic day biases (Fig. 5b) were calculated using 12 successful comparison flights of each type to 26 km, 12 flights to 32 km, and 10 flights to 33 km. The reference for the systematic bias plots (Figs. 5a and 5b) were four independent sensor types with good time constants of response at all heights.

a. Nighttime performance during 2010 WMO intercomparison

Figure 5a shows the systematic bias of the 11 systems between simultaneous temperature measurements during the night. Below the tropopause (around 16 km) systematic differences of all systems are within more or less ±0.2°C. Around the tropopause larger differences are observed on some sensors, which is likely linked to icing effects on the sensors when they leave dense upper clouds. At higher altitudes in the stratosphere, the differences are around ±0.4°C. Overall, these results are rather good, particularly if we take into account that the increase from ±0.2° to ±0.4°C in the upper part is mainly due to three systems with larger biases. The Meteolabor system shows an interesting behavior, with the highest temperature in the troposphere and among the coldest in the stratosphere. This fact is further investigated below in the context of radiative cooling in the lower troposphere and radiative warming in the stratosphere observed during nighttime (Fig. 4b).

b. Daytime performance during 2010 WMO intercomparison

Daytime systematic differences of simultaneous temperature measurements are on the order of ±0.4°C in the troposphere and around ±0.8°C in the stratosphere (Fig. 5b). The large divergence, particularly in the stratosphere, is primarily due to the solar radiation error, which strongly increases because of the reduced atmospheric pressure and related ventilation. The Meteolabor system shows a large cold bias, which is due to a very large radiation correction of about −1.8°C around

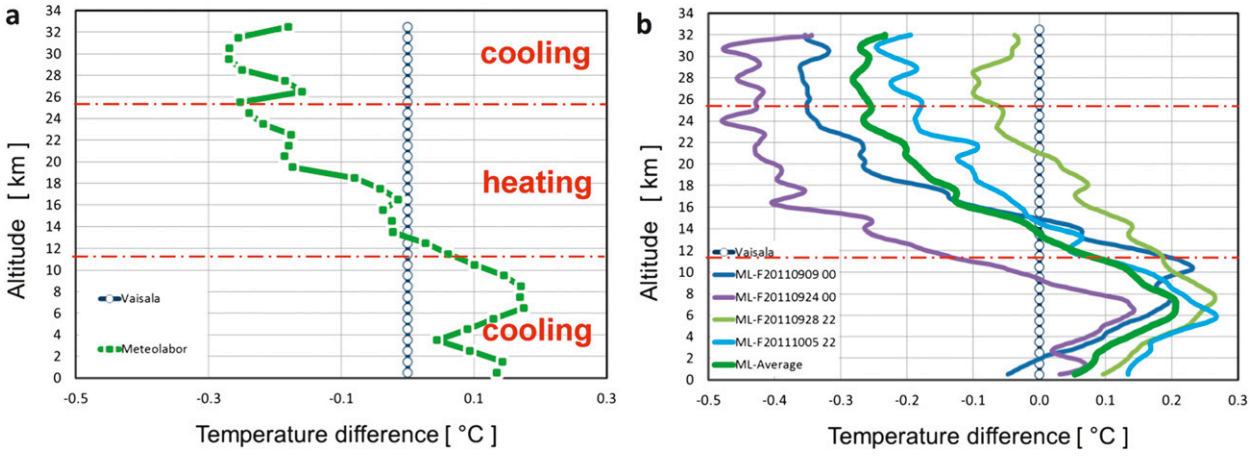

FIG. 6. Nighttime temperature difference Meteolabor minus Vaisala with Vaisala as reference (a) average reported during the 2010 WMO radiosonde intercomparison and (b) measured in four flights at Payerne in 2011.

30-km altitude. This large cold bias was the main motivation for the present reinvestigation of the radiation error on the Meteolabor temperature sensor.

6. Nighttime thermal radiation error

Figure 4b shows that the thermal radiation balance of temperature sensors at night suggests a cooling of the sensor in the lower troposphere and a warming in the upper troposphere and lower stratosphere. Above 25-km altitude, the warming again switches to a cooling.

a. Temperature sensor size

The analysis of gas temperature measurements showed that the sensor size, its surface emissivity–absorptivity, and its ventilation are the three most critical parameters with respect to measurement errors. The ventilation, even though strongly changing with altitude, is more or less the same in all experiments since the ascent rate of radiosondes is always on the order of 5 m s^{-1}. Emissivity–absorptivity is not well known for the individual sensors. However, the sensor size can be measured and allows best to quantify the thermal emission–absorption of the individual sensors. With its 64-μm copper and 50-μm constantan wires, the Meteolabor sonde has the smallest temperature sensor of all the radiosonde systems used in the 2010 WMO intercomparison.

b. Nighttime temperature differences between Meteolabor and Vaisala

In Fig. 6a we show temperature differences between the Meteolabor and the Vaisala systems during the 2010 WMO intercomparison in China. With the Vaisala taken as reference, we observe that the Meteolabor sensor measures too high a temperature in the troposphere and too low a temperature in the stratosphere. To show that this behavior is not only observed in tropical latitudes, we show similar comparisons between Meteolabor and Vaisala at midlatitudes, made at the station Payerne during 2011. Figure 6b shows four individual flights and the average, which show a very similar pattern with Meteolabor warmer in the troposphere and colder in the stratosphere by similar amounts as during the 2010 WMO intercomparison. The Vaisala temperature sensor, which is about 200 μm thick, has a diameter about 3 times larger than the Meteolabor sensor. With a thermal cooling tendency in the troposphere, the larger Vaisala sensor likely reacted stronger to cooling, and accordingly stronger to thermal heating in the stratosphere.

7. Daytime thermal and solar radiation error

Thermal longwave radiation produces similar errors on temperature sensors during the day and during the night (Fig. 4c). In the troposphere these errors are on the order of 0.1°C on the Meteolabor sensor and may be compensated by solar radiation. In the stratosphere, however, solar radiation errors are considerably larger than thermal errors. Important to note is that above the tropopause, direct solar radiation and surface-reflected solar radiation are more or less constant.

a. Measuring the solar radiation error

The experimental setup for direct in situ measurements of the radiation error is shown in Fig. 3 and described in chapter 3b. The basic idea is to measure air

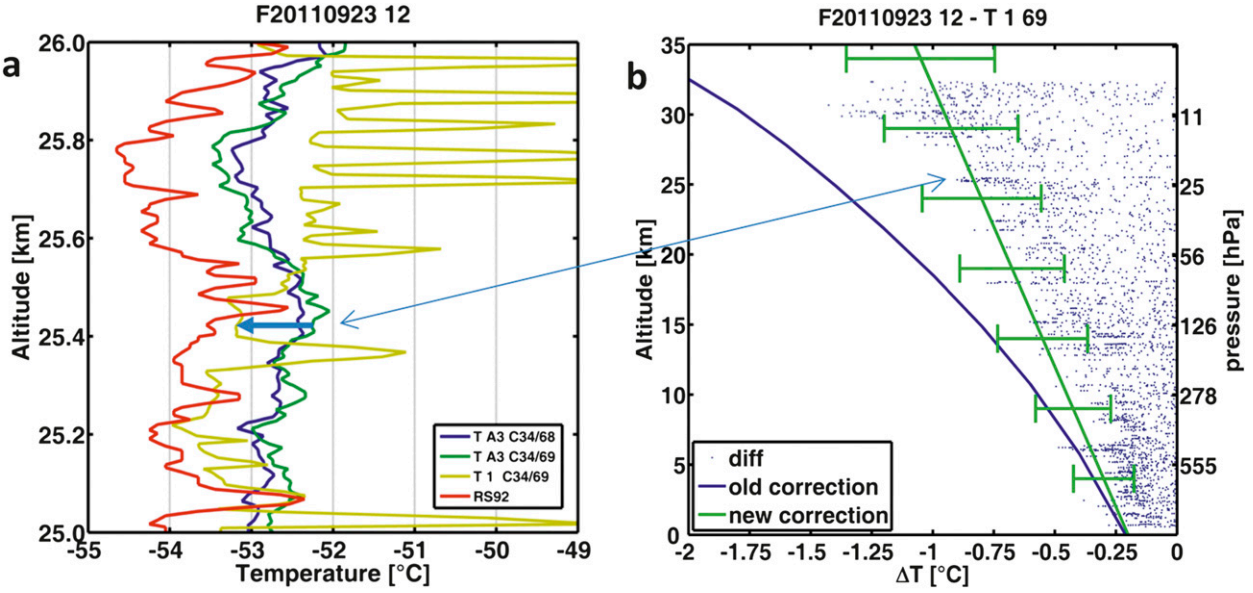

FIG. 7. (a) Measurements of four temperature sensors between 25- and 26-km altitude. TA3 C34/68 and TA3 C34/69 are sun-exposed uncorrected temperature measurements of two Meteolabor radiosondes. T1 C34/69 is an additional temperature sensor at a distance of 5 cm from the shading plate. RS92 is a solar-corrected temperature measurement of a Vaisala radiosonde. (b) Difference of T1 C34/69 minus TA3 C34/69 for all altitudes [also shown by the blue arrow in (a)]. Old (blue) and the new (green) radiation correction curves are shown.

temperature during special radiosonde ascents with the operational all-time sun-exposed sensor, and to compare these measurements with identical air sensors that are at times unshaded and at times shaded by a shading plate mounted on the radiosonde.

Data measured during a more or less cloud-free noontime flight on 23 September 2011 is shown as an example in Fig. 7. To explain the measurement principle, we show the temperature measured by four sensors between 25- and 26-km altitude (Fig. 7a). Two operational all-time sun-exposed temperature measurements from two different Meteolabor sondes—TA3 C34/68 (blue) and TA3 C34/69 (green)—show the uncorrected air temperature with an average difference of about 0.2°C between the two sondes. T1 C34/69 (yellow) is one of the sensors that is located at a distance of 5 cm from the center of the shading plate. Between 25.1 and 25.5 km, T1 C34/69 is about 0.8°C colder than the operational sun-exposed TA3 C34/69 sensor (both sensors are of the same sonde C34/69). Here we observe that during this phase, T1 C34/69 was mostly shaded by the shading plate. Above 25.5 km we observe that T1 C34/69 is getting warmer than TA3 C34/69; hence, during this phase the sensor is unshaded. During this phase, with the sensor in front of the shading plate and exposed to the sun, temperature spikes of several degrees above the operational sun-exposed sensor temperature are observed. These spikes are not fully understood, but are very different from the behavior of the temperature reading of the operational sensors (with no shading plate behind) and the temperature readings of the sun-shaded sensor. Temperature measurements of the shading plate itself showed that the size of the spikes that appeared in front of the plate were related to the plate color and hence the plate temperature, whereas no plate color and temperature dependence was found on the temperature measured in the shade of the plate. From these measurements we conclude that the temperature measured by T1 C34/69 is the real true temperature reading whenever the sensor is shaded by the plate. The red curve is the solar-radiation-corrected temperature measured by the Vaisala RS92-SGP sonde. We observe that around 25.2 km when T1 C34/69 is shaded, the RS92-SGP shows about 0.2°C colder. The measurements also show that the sonde rotation (which is the same for all sondes) produces larger temperature variations on the Vaisala RS92-SGP than on the two Meteolabor TA3 sensors.

b. *Solar radiation correction*

The analysis over the entire altitude range is made by calculating the difference between the shaded T1 C34/69 measurement minus the sun-exposed TA3 C34/69 measurement (blue arrow shown in Fig. 7a). These differences are shown in Fig. 7b, with dots representing measurements taken each second when T1 was colder than TA3. The coldest temperatures measured under

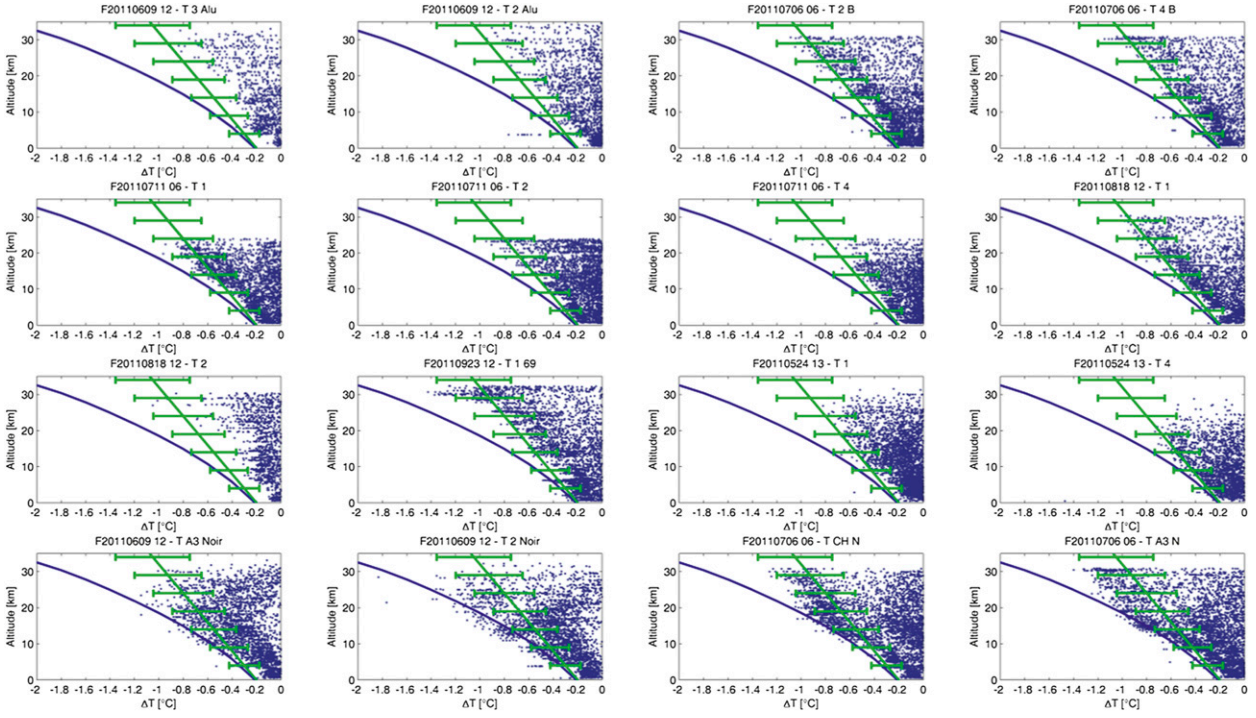

FIG. 8. Temperature difference between shaded sensors located close to the shading plate minus unshaded temperature sensor, during eight individual flights (blue dots). Green line curve represents the new radiation correction curve with an uncertainty of ±0.1°C at the surface and ±0.3°C at 32-km altitude. Old correction curve is shown in blue.

shaded conditions are then assumed to represent the correct air temperature measurement. The figure shows that the old solar radiation error curve (blue polynomial curve) is outside the blue dots and hence too large, particularly in the stratosphere. A new solar radiation error curve (green linear line) has therefore been determined using measurements from 16 sensors, which were shaded–unshaded during eight individual flights (Fig. 8). The new curve represents an average solar error, following the coldest temperatures observed during the 16 measurements, and assuming a linear increase and an uncertainty of ±0.1°C at the surface and ± 0.3°C at 32-km altitude. The uncertainty is based on the variations over the 16 measurements, which were made under different atmospheric conditions. In the troposphere the uncertainty is strongly influenced by varying cloud conditions, and in the stratosphere it strongly depends on the reflection of the clouds below.

The old radiation error curve (Fig. 7, blue) was calculated with respect to atmospheric pressure as a mean temperature difference ΔT_{year} profile for the whole year and was represented by the second-degree polynomial fit (Ruffieux and Joss 2003):

$$\Delta T_{\text{year}} = 2.927 - 1.293\log(p) + 0.131[\log(p)]^2. \qquad (1)$$

The new radiation error curve (Fig. 7, green) or mean temperature difference ΔT_{year} profile for the whole year, on the other hand, is represented as a first-order linear equation with respect to geopotential altitude:

$$\Delta T_{\text{year}} = 0.2 + \left(0.8\frac{\text{Alt geo}}{32'000}\right). \qquad (2)$$

Equation (2) is now used for the radiation correction of all 1200 UTC flights made with the new digital Meteolabor SRS-C34 radiosonde at Payerne. The equation has also been used to correct all measurements made with the SRS-C34, since its introduction as operational radiosonde in January 2011. Measurements that were made with the old analog radiosonde SRS-400 from 1990 to the end of 2010 have also been corrected in the Data Warehouse (DWH) of MeteoSwiss. The old analog and the new digital radiosondes from Meteolabor use basically the same copper–constantan thermocouple sensor, except for the physical connection of the thin copper and constantan wires, which was X shaped on the SRS-400 and is now V shaped on the SRS-C34. Weekly double soundings between the old SRS-400 and the new SRS-C34 during 2011 revealed that X-shaped sensors had a slightly larger radiation error than the new V-shaped sensors, and therefore the following slightly modified

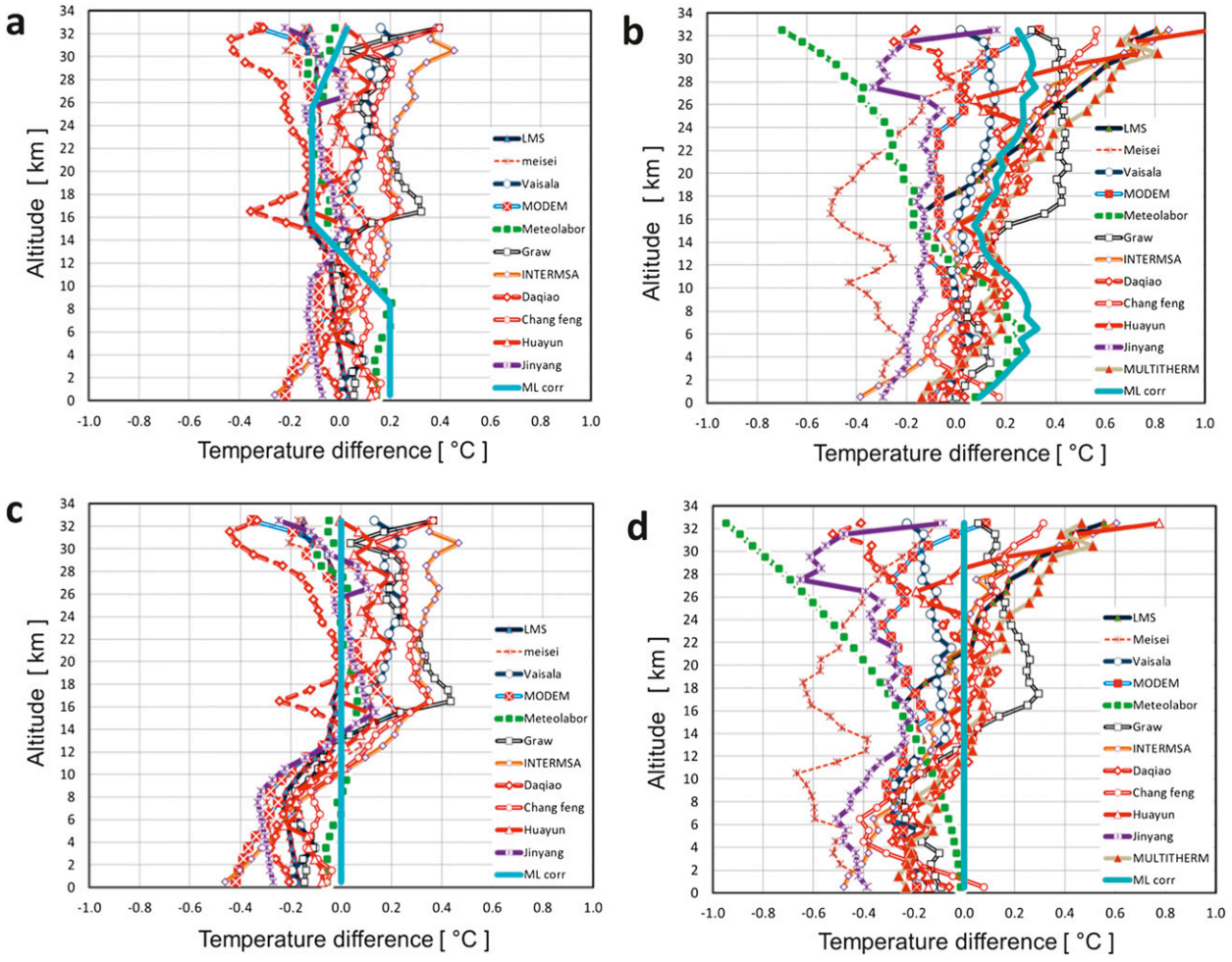

FIG. 9. Thermal and solar radiation corrections applied on Meteolabor measurements taken during the 2010 WMO radiosonde intercomparison in Yangjiang, China: (a) night and (b) day. WMO intercomparison results referenced to new Meteolabor corrections: (c) night and (d) day.

equation was used to correct all the old soundings made with the SRS-400:

$$\Delta T_{\text{year}} = 0.2 + \left(1.1\frac{\text{Alt geo}}{32'000}\right). \quad (3)$$

8. New thermal and solar radiation error curves

The radiation profiles show that thermal longwave radiation upward and downward have cooling and warming effects on temperature sensors. The Meteolabor thermocouple, being the smallest temperature sensor, is likely less influenced than other sensors, but it is too cold in the lower troposphere and too warm in the UTLS. Nevertheless, so far no thermal radiation error corrections are made on the Meteolabor temperature sensor, neither on the old SRS-400 nor on the new SRS-C34 night measurements.

However, since the present analysis suggests minor corrections for night measurements, we are adding here longwave corrections on the Meteolabor night measurement during the 2010 WMO intercomparison (Fig. 9a), assuming that the correct reading would be slightly warmer in the troposphere, slightly colder in the UTLS, and again slightly warmer in the stratosphere.

Solar radiation errors, on the other hand, are corrected on all measurements using Eq. (2) and are also applied on daytime measurements of the 2010 WMO intercomparison results shown in Fig. 9b. In the troposphere the Meteolabor reading is still the warmest of all sensors, even though only solar correction has been applied. This suggests that it is likely that all other operational radiosondes measure too cold in the troposphere. In the stratosphere the new correction curve brings the Meteolabor sensor in between the other radiosondes used during the 2010 WMO intercomparison.

9. Results and conclusions

Thermal longwave and solar shortwave radiation profiles allowed determining the radiation balance on temperature sensors during the night and day. The nighttime longwave radiation balance suggests cooling and heating at different altitudes, and suggests corrections of temperature sensors on the order of ±0.2°C. Figure 9c shows the 2010 WMO intercomparison results referenced to thermal-radiation-corrected nighttime Meteolabor readings. Radiative cooling in the lower troposphere apparently led to a cold bias of −0.2° ± 0.2°C for all radiosondes compared to Meteolabor. In the UTLS and in the stratosphere, radiative heating produces a warm bias of +0.2° ± 0.2°C for many radiosondes. Further experimental investigations will have to be made on this issue.

Solar shortwave radiation errors were determined using Meteolabor thermocouples under shaded and unshaded conditions during the flight. These results led to an experimental determination of the solar radiation error. Figure 9d shows the 2010 WMO intercomparison results referenced to Meteolabor results, which are corrected with the new solar radiation error curve. In the lower troposphere the measurements of all radiosonde systems are −0.2° ± 0.2°C colder than Meteolabor measurements, which is likely due to thermal and solar radiation errors. However, in the stratosphere the new radiation correction centers the Meteolabor system within the results of the majority of the other radiosonde systems. The differences in the troposphere will have to be further analyzed, and future international intercomparisons will help to reduce differences between radiosonde temperature measurements.

Acknowledgments. Rolf Philipona directed the experiments, made the analyses, and wrote the manuscript. Andreas Kräuchi provided new technology for flying, tracing, and recovering the payload of the special balloon flights. Gonzague Romanens, Gilbert Levrat, and Emmanuel Brocard helped to launch, track, and recover the special sondes. Paul Ruppert provided the knowledge on thermocouple measurements and helped with the analyses. Pierre Jeannet checked the results and applied the new radiation correction on previous measurements. Dominique Ruffieux and Bertrand Calpini participated in many discussions and various tasks. All authors reviewed the manuscript. The authors would like to acknowledge the radiosonde group of the Payerne aerological station for helping to launch the special radiosondes for these particular experiments.

REFERENCES

Daniels, G. E., 1968: Measurements of gas temperature and the radiation compensating thermocouple. *J. Appl. Meteor.,* **7,** 1026–1035.

Freeze, P. D., 1951: Bibliography on the measurement of gas temperatures. National Bureau of Standards Circular 513, U.S. Government Printing Office, 14 pp.

GCOS, 2007: GCOS Reference Upper-Air Network (GRUAN): Justification, requirements, siting and instrumentation options. GCOS-112, WMO/TD-1379, 25 pp.

——, 2010: Implementation plan for the global observing system for climate in support of the UNFCCC (2010 update). GCOS-138, GOOS-184, GTOS-76, WMO/TD-1523, 179 pp.

Luers, J. K., 1990: Estimating the temperature error of the radiosonde rod thermistor under different environments. *J. Atmos. Oceanic Technol.,* **7,** 882–895.

——, 1997: Temperature error of the Vaisala RS90 radiosonde. *J. Atmos. Oceanic Technol.,* **14,** 1520–1532.

McMillin, L., M. Uddstrom, and A. Coletti, 1992: A procedure for correcting radiosonde reports for radiation errors. *J. Atmos. Oceanic Technol.,* **9,** 801–811.

Nash, J., T. Oakley, H. Vömel, and L. I. Wei, 2011: WMO intercomparion of high quality radiosonde systems: Yanjiang, China, 12 July–3 August 2010. IOM Rep. 107, WMO/TD-1580, 238 pp.

Philipona, R., A. Kräuchi, and E. Brocard, 2012: Solar and thermal radiation profiles and radiative forcing measured through the atmosphere. *Geophys. Res. Lett.,* **39,** L13806, doi:10.1029/2012GL052087.

Randel, W. J., F. Wu, H. Vömel, G. E. Nedoluha, and P. Forster, 2006: Decreases in stratospheric water vapor after 2001: Links to changes in the tropical tropopause and the Brewer-Dobson circulation. *J. Geophys. Res.,* **111,** D12312, doi:10.1029/2005JD006744.

Ruffieux, D., and J. Joss, 2003: Influence of radiation on the temperature sensor mounted on the Swiss radiosonde. *J. Atmos. Oceanic Technol.,* **20,** 1576–1582.

Schmidlin, F., J. K. Luers, and P. D. Huffman, 1986: Preliminary estimates of radiosonde thermistor errors. NASA Tech. Paper 2637, 15 pp.

Seidel, D. J., and Coauthors, 2009: Reference upper-air observations for climate: Rationale, progress, and plans. *Bull. Amer. Meteor. Soc.,* **90,** 361–369.

Thorne, P. W., D. E. Parker, J. R. Christy, and C. A. Mears, 2005: Uncertainties in climate trends: Lessons from upper-air temperature records. *Bull. Amer. Meteor. Soc.,* **86,** 1437–1443.

Trenberth, K. E., T. R. Karl, and T. W. Spence, 2002: The need for a systems approach to climate observations. *Bull. Amer. Meteor. Soc.,* **83,** 1558–1559.

Väisälä, V., 1964: An analysis of the radiation error appearing in temperature measurements made with radiosondes. *Ann. Acad. Sci. Fenn. Ser. A6,* **158,** 3–24.